Cascaded Control System of the Modular Multilevel Converter for Feeding Variable-Speed Drives

Johannes Kolb, Felix Kammerer, Mario Gommeringer, and Michael Braun

***Abstract*—The modular multilevel converter (MMC) is an upcoming topology for high-power drive applications especially in the medium voltage range. This paper presents the design process of a holistic control system for a MMC to feed variable-speed drives. First, the design of the current control for the independent adjustment of several current components is derived from the analysis of the equivalent circuits. Second, the current and voltage components for balancing the energies in the arms of the MMC are identified systematically by the investigation of the transformed arm power components. These fundamentals lead to the design of the cascaded control structure, which allows the balancing task in the whole operating range of a three-phase machine. The control system ensures a dynamic balancing of the energies in the cells of the MMC at minimum necessary internal currents over the complete frequency range. Simultaneously, all other circulating current components are avoided to minimize current stress and additional voltage pulsations. The performance of the control system is finally validated by measurements on a low-voltage MMC prototype, which feeds a field-oriented controlled induction machine.**

***Index Terms*—Control theory, modular multilevel converter (MMC), variable-speed drives.**

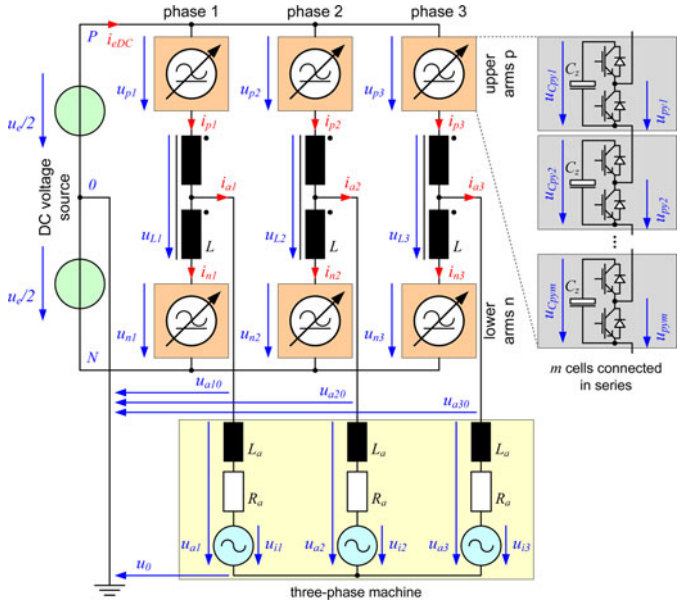

Fig. 1. Schematic of the MMC with the definitions of voltages and currents.

I. Introduction

THE modular multilevel converter (MMC) was introduced in 2002 [1] as dc–3ac configuration for high-voltage dc power transmission. The use of this topology for feeding electrical drives in the range of medium voltage was proposed in [2] and [3]. First, experimental results with low-voltage prototypes of MMC-based drive converters are shown in [4] and [5]. The most challenging issue of operating the MMC at low frequency, which is necessary for variable-speed drives, was first solved in [6]. The increasing amount of the energy pulsation in the capacitors of the cells at low frequencies or even standstill is reduced to acceptable values by the use of an ac common-mode voltage with corresponding inner currents. An appropriate control scheme, especially for this low-frequency mode, is presented in [7] and [8]. Here, a cascaded structure with subordinated current control loops and filter-based energy control loops is proposed. The optimization of the modulation [9] as well as the dimensioning process of the MMC [10] allow an efficient and high dynamic operation of the MMC for feeding three-phase machines. In [10] and [11], experimental results based on this control scheme and optimizations are shown. For an operation at nominal torque of the machine even at low frequencies, see [12], the MMC has to be overdimensioned with respect to the additional current stress of the inner balancing currents compared to the operating point at nominal speed. The authors of [12] proposed a new method for reducing the energy pulsation in the range of intermediate-speed and present extensive measuring results of steady-state operations at different frequencies. A further improvement for reducing the peak values of the inner currents by using square-wave currents for the balancing task is shown in [13]. This method causes large ac-contents in the dc voltage respectively in the dc current. A dynamic control of the MMC for feeding electric drives is proposed in [14] and demonstrated by experimental results. However, in [12]–[14], no waveform of the dc current is shown, which is also an important aspect regarding additional current stress of the dc-voltage source due to a possible harmonic content.

A. Structure, Fundamentals, and Definitions of the MMC

The complete system including the dc-voltage source, the MMC itself, and the three-phase machine is illustrated in Fig. 1 [11]. The MMC includes three phases, each with an upper arm

Manuscript received September 30, 2013; revised November 28, 2013; accepted December 23, 2013 Date of publication January 13, 2014; date of current version August 26, 2014. Recommended for publication by Associate Editor Prof. M. Saeedifard.

The authors are with the Elektrotechnisches Institut, Karlsruhe Institute of Technology, 76131 Karlsruhe, Germany (e-mail: johannes.kolb@partner.kit.edu; felix.kammerer@kit.edu; mario.gommeringer@kit.edu; michael.braun@kit.edu).

Color versions of one or more of the figures in this paper are available online at http://ieeexplore.ieee.org.

Digital Object Identifier 10.1109/TPEL.2014.2299894

p and a lower arm n. The currents in the arms are defined as i_{xy} (upper or lower arm: $x \in \{p,n\}$, no. of phase: $y \in \{1,2,3\}$). One converter arm is built by m cells (no. of cell: $z \in \{1 \cdots m\}$) connected in series plus a coupled inductor L. One cell of this dc–3ac configuration consists of a single half bridge with a capacitor C_z. By switching the half bridges of the cells, each arm is able to generate an adjustable arm voltage u_{xy} with $m+1$ voltage steps. Due to the half bridges in the cells and a pulse-width modulation (PWM) of at least one cell, the range of the specific arm voltage is

$$0 \le u_{xy} = \sum_{z=1}^{m} u_{xyz} \le u_{Cxy} = \sum_{z=1}^{m} u_{Cxyz}. \tag{1}$$

Here, u_{Cxy} is the sum of the capacitors' voltages of all cells in the arm xy. These voltages u_{Cxy} correspond to the arm energies w_{xy} which are stored in the capacitors C_z of each arm. Both can be separated into constant components ($\bar{u}_C$, $\bar{w}_C$), which have to be equal in each arm, and the individual time-variant parts $\tilde{u}_{Cxy}$ and $\tilde{w}_{xy}$. The time-variant arm energies $\tilde{w}_{xy}(t)$ are determined by the integration of the arm power p_{xy} assuming that the balancing task will ensure constant arm energies $\bar{w}_C$

$$\tilde{w}_{xy}(t) = \int_0^t \underbrace{u_{xy}(\tau) \cdot i_{xy}(\tau)}_{=p_{xy}(\tau)} \partial\tau. \tag{2}$$

Hence, the components of the capacitor voltages and the corresponding arm energies become equal by

$$u_{Cxy}^2(t) = \left(\bar{u}_C + \tilde{u}_{Cxy}(t)\right)^2 = \frac{2m}{C_z} \cdot \underbrace{(\bar{w}_C + \tilde{w}_{xy}(t))}_{=w_{xy}(t)}. \tag{3}$$

On the three-phase ac side, the MMC generates the phase voltages u_{ay0} related to the midpoint 0 of the dc source. The common-mode voltage u_0 of the neutral point of the three-phase machine is also related to the reference potential of the dc-voltage source. The phase voltages u_{ay0} as well as the phase currents i_{ay} are transformed to the $\alpha\beta 0$-components of the corresponding space vectors by the Clarke-transformation of (43)

$$\begin{bmatrix} u_{a\alpha} \\ u_{a\beta} \\ u_0 \end{bmatrix} = \mathbf{C} \cdot \begin{bmatrix} u_{a10} \\ u_{a20} \\ u_{a30} \end{bmatrix} \quad \begin{bmatrix} i_{a\alpha} \\ i_{a\beta} \\ i_{a0} \end{bmatrix} = \mathbf{C} \cdot \begin{bmatrix} i_{a1} \\ i_{a2} \\ i_{a3} \end{bmatrix}. \tag{4}$$

These Cartesian components could also be expressed by their polar coordinates ($\hat{u}_a$, $\hat{i}_a$: amplitudes of voltages and currents, respectively, γ_a: phase angle of three-phase voltage, φ_a: phase difference of voltage and current)

$$u_{a\alpha} = \hat{u}_a \cdot \cos(\gamma_a) \quad i_{a\alpha} = \hat{i}_a \cdot \cos(\gamma_a - \varphi_a) \tag{5}$$

$$u_{a\beta} = \hat{u}_a \cdot \sin(\gamma_a) \quad i_{a\beta} = \hat{i}_a \cdot \sin(\gamma_a - \varphi_a). \tag{6}$$

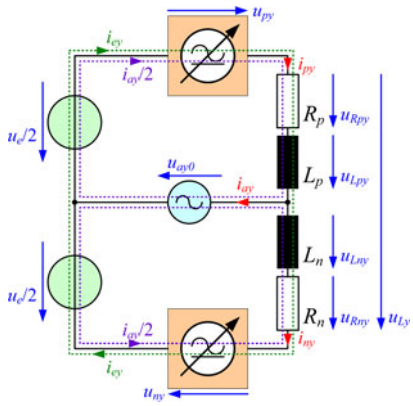

Fig. 2. Equivalent circuit of one phase of the MMC.

II. Decoupled Current Control of the MMC

A. Analysis and Transformation of the MMC Network

Each arm current i_{xy} consists of the components belonging to the dc side i_{ey} and half of the phase current i_{ay} (see Fig. 2)

$$i_{py} = i_{ey} + \frac{i_{ay}}{2} \quad i_{ny} = i_{ey} - \frac{i_{ay}}{2}. \tag{7}$$

The differential equations of i_{ey} and i_{ay} follow from the analysis of the equivalent circuit of one phase of the MMC in Fig. 2, see [7], [8], and [15]

$$\dot{i}_{ey} = \frac{1}{2L} \cdot (u_e - u_{py} - u_{ny} - 2R \cdot i_{ey}) \tag{8}$$

$$\dot{i}_{ay} = \frac{1}{L} \cdot (-2u_{ay} - u_{py} + u_{ny} - R \cdot i_{ay}). \tag{9}$$

The impedances of the p- and n-arms are assumed to be equal ($R = R_p = R_n$, $L = L_p = L_n$).

The transition from the single-phase equations according to (8) and (9) to the transformed three-phase system of the MMC is performed by expressing the six-arm voltages u_{xy} and the current components i_{ey} of the dc side by their $\alpha\beta 0$-components from the Clarke-transformation

$$\begin{bmatrix} u_{x\alpha} \\ u_{x\beta} \\ u_{x0} \end{bmatrix} = \mathbf{C} \cdot \begin{bmatrix} u_{x1} \\ u_{x2} \\ u_{x3} \end{bmatrix} \quad \begin{bmatrix} i_{e\alpha} \\ i_{e\beta} \\ i_{e0} \end{bmatrix} = \mathbf{C} \cdot \begin{bmatrix} i_{e1} \\ i_{e2} \\ i_{e3} \end{bmatrix}. \tag{10}$$

Replacing the arm voltages and the e-currents in (8) by these $\alpha\beta 0$-components yields to the following differential equations, which are illustrated as equivalent circuits in Fig. 3:

$$\begin{bmatrix} \dot{i}_{e\alpha} \\ \dot{i}_{e\beta} \\ \dot{i}_{e0} \end{bmatrix} = \mathbf{C} \cdot \begin{bmatrix} \dot{i}_{e1} \\ \dot{i}_{e2} \\ \dot{i}_{e3} \end{bmatrix} = \frac{1}{2L} \begin{bmatrix} -u_{p\alpha} - u_{n\alpha} - 2R \cdot i_{e\alpha} \\ -u_{p\beta} - u_{n\beta} - 2R \cdot i_{e\beta} \\ u_e - u_{p0} - u_{n0} - 2R \cdot i_{e0} \end{bmatrix}. \tag{11}$$

The same procedure is performed with the currents at the 3ac side of (9) by the use of the transformation of the phase values

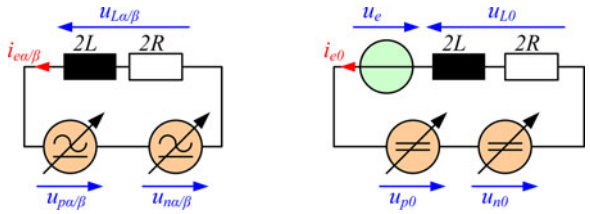

Fig. 3. Resulting equivalent circuits of the transformed e-current components.

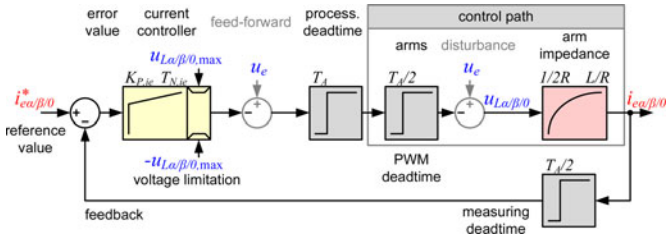

Fig. 4. Current control loops of the e-currents in transformed components.

according to (4)

$$\begin{bmatrix} u_{a\alpha} \\ u_{a\beta} \\ u_0 \end{bmatrix} . = \frac{1}{2} \begin{bmatrix} -u_{p\alpha} + u_{n\alpha} - R \cdot i_{a\alpha} - L \cdot \dot{i}_{a\alpha} \\ -u_{p\beta} + u_{n\beta} - R \cdot i_{a\beta} - L \cdot \dot{i}_{a\beta} \\ -u_{p0} + u_{n0} \end{bmatrix} . \quad (12)$$

The voltages $-L \cdot \dot{i}_{a\alpha/\beta}$ will be zero if magnetically coupled inductors are used in the phases of the MMC (see Fig. 1). The voltage drops of the resistance $-R \cdot i_{a\alpha/\beta}$ are neglected. They will be compensated by the current controllers of $i_{a\alpha/\beta}$.

B. Voltage Components for the Current Control

The voltages across the impedances are summarized to the three control voltages $u_{L\alpha/\beta/0}$ of the corresponding e-currents, see Fig. 3

$$u_{L\alpha/\beta/0} = 2L \cdot \dot{i}_{e\alpha/\beta/0} + 2R \cdot i_{e\alpha/\beta/0}. \quad (13)$$

These control voltages allow a specific and independent adjustment of the internal currents $i_{e\alpha}$ and $i_{e\beta}$ (often denoted as circulating currents) as well as the current of the dc-side $i_{e\mathrm{DC}}$. This current corresponds to the zero sequence component i_{e0}, which is the mean value of all six-arm currents, by $i_{e\mathrm{DC}} = 3i_{e0}$. The composition of the six-arm voltages u_{xy} is achieved by solving the system of equations of (11) and (12). The inverse transformation of the $\alpha\beta 0$-components of the p- and n-arms yields to the reference values of the arm voltages

$$\begin{bmatrix} u^*_{p1} \\ u^*_{p2} \\ u^*_{p3} \end{bmatrix} = \mathbf{C}^{-1} \cdot \begin{bmatrix} -\frac{1}{2}u_{L\alpha} - u_{a\alpha} \\ -\frac{1}{2}u_{L\beta} - u_{a\beta} \\ \frac{1}{2}u_e - \frac{1}{2}u_{L0} - u_0 \end{bmatrix} \quad (14)$$

$$\begin{bmatrix} u^*_{n1} \\ u^*_{n2} \\ u^*_{n3} \end{bmatrix} = \mathbf{C}^{-1} \cdot \begin{bmatrix} -\frac{1}{2}u_{L\alpha} + u_{a\alpha} \\ -\frac{1}{2}u_{L\beta} + u_{a\beta} \\ \frac{1}{2}u_e - \frac{1}{2}u_{L0} + u_0 \end{bmatrix} . \quad (15)$$

These six reference values have to be converted to the corresponding switching states for the cells by the modulator, which has to include the energy balancing of the cells inside of each arm [7], [10], [16], see Figs. 5 and 7.

This approach enables, in addition to the decoupled control of the internal currents $i_{e\alpha/\beta}$ and the dc current i_{e0} / $i_{e\mathrm{DC}}$, the independent and individual adjustment of the three-phase current system $i_{a\alpha/\beta}$ by the corresponding voltage system $u_{a\alpha/\beta}$, see (12).

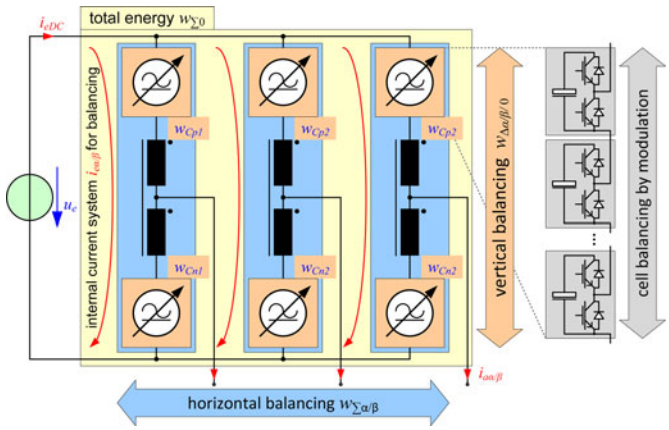

Fig. 5. Energy control and balancing tasks in the MMC.

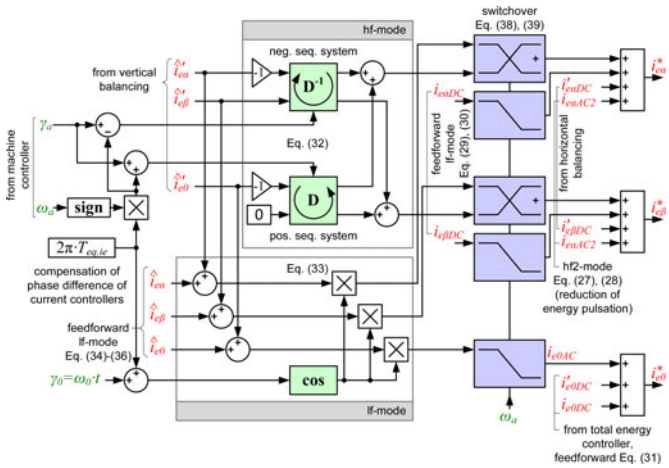

Fig. 6. Estimation of the e-current reference values.

The common-mode voltage u_0 can be freely adjusted within the limits of the arm voltages u_{xy}, which depend on the instantaneous sum of the capacitor voltages u_{Cxy}, see (1). It consists of two components

$$u_0 = \underbrace{-\frac{1}{6}\hat{u}_a \cdot \cos(3\gamma_a)}_{=u_{0a}} + \underbrace{\hat{u}_0 \cdot \cos(\omega_0 \cdot t)}_{=u_{0e}} . \quad (16)$$

The part u_{0a} is used for increasing the output voltage by factor $2/\sqrt{3}$ with the third harmonic of γ_a for the overmodulation. The part u_{0e} is used as degree of freedom for the balancing task at low-frequency operation [6], [7], which is described later. Here, an ac component with the amplitude $\hat{u}_0$ and an arbitrary frequency ω_0 is set.

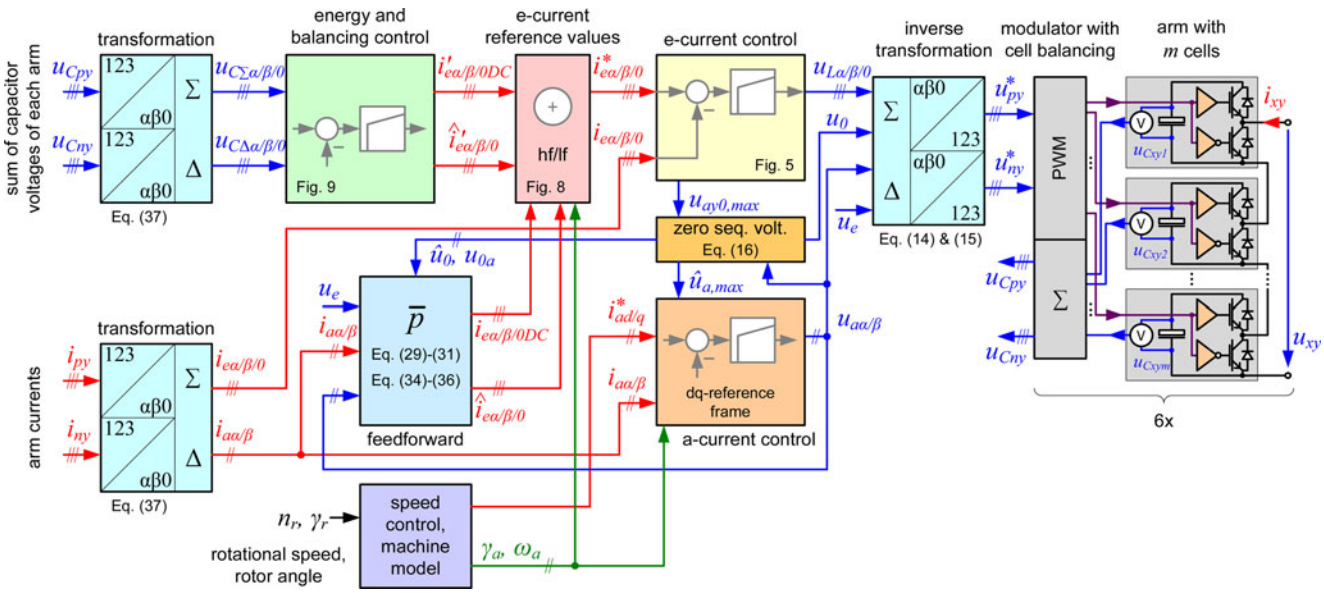

Fig. 7. Signal flow path of complete MMC control system with subordinate current controllers, arm energy balancing, motor control unit, and modulator.

C. Function of the Arm Inductances

The inductances L decouple the six voltage sources realized by the arms of the MMC. In this approach, the inductances allow the individual adjustment of the several currents by the respective current control loops with the voltage components of (12) and (13). In [2] and [17], it is proposed to use the inductance for damping the internal currents in the range of the output frequency. This feature is not necessary by using the presented decoupled current control, because only the desired internal currents are adjusted and the arm voltages u_{xy} are independently generated by the modulator [7], [10], [16]. Therefore, the inductance L has to be dimensioned on the basis of the switching states of the cells and accordingly with the modulation scheme. In [10], the design process of the inductance is described in detail. To sum up, the inductance L is determined by the maximum allowed ripple content of the dc and inner currents Δi_{ey}. It depends on the switching frequency f_{PWM} of the PWM, if one cell per arm and switching cycle is modulated, and on the cell voltage u_{Cxyz}. Consequently, the value of the inductance L is determined by the voltages on the level of the cells and not by the voltages or currents of the arms. This yields to a relative small value of the inductance L. To change the desired currents i_{e0} and $i_{e\alpha/\beta}$ in the control loops, only small voltage components are necessary. Because of this, the parts of $u_{L\alpha/\beta/0}$ are neglected in Section III-A.

D. Current Control Loops of the MMC

The three current control loops, see Fig. 4, for $i_{e\alpha}$, $i_{e\beta}$, and i_{e0} are derived by the equivalent circuits of Fig. 3 and their equations (11). Each control loop incorporates the impedances (L, R) of the arms, in which the current components have to be controlled by the corresponding voltages $u_{L\alpha}$, $u_{L\beta}$, and u_{L0}, see Fig. 3. The measured value of the dc voltage u_e is used as feedforward in the control loop of i_{e0}, see Fig. 4. Each current controller is realized by a time-discrete P- or PI-controller (P: proportional, I: integral) with the sampling time T_A. The dead times of the measurement, signal processing, and PWM are included by the sum of the small time constants $T_{\sigma,ie} = 2T_A$. Then, the maximum gain of the proportional part of the controller is [18]

$$K_{P,ie} = \frac{T_{S,ie}}{2V_{S,ie} \cdot T_{\sigma,ie}} = \frac{\frac{L}{R}}{\frac{2}{2R} \cdot 2T_A} = \frac{L}{2T_A}. \tag{17}$$

$V_{S,ie} = 1/2R$ is the gain of the control path and $T_{S,ie} = L/R$ the corresponding time constant. Due to the fact, that the energy controllers will be superposed, a P-controller will be sufficient. The I-part of the current controller could be used especially for the dc-current i_{e0} for compensating the time constant $T_{N,ie} = T_{S,ie} = L/R$. Consequently, the dynamic behavior of the closed control loops corresponds approximately to a first-order time-delay element with the equivalent time constant $T_{\mathrm{eq,ie}} = 2T_{\sigma,ie} = 4T_A$.

III. Balancing of the Arm Energies

A. Transformation of Arm Power Components

For the balancing of the six-arm energies w_{xy}, the values of the corresponding arm power p_{xy} are transformed comparable to Section II-A. First, the upper and lower power components are converted to their mean value and difference

$$p_{\Sigma y} = \frac{1}{2}(p_{py} + p_{ny}) \quad = \frac{1}{2}(u_{py} i_{py} + u_{ny} i_{ny}) \tag{18}$$

$$p_{\Delta y} = p_{py} - p_{ny} \quad = u_{py} i_{py} - u_{ny} i_{ny}. \tag{19}$$

Second, these power components are transformed by the Clarke matrix $\mathbf{C}$ to the $\alpha\beta 0$-components

$$\begin{bmatrix} p_{\Sigma\alpha} \\ p_{\Sigma\beta} \\ p_{\Sigma 0} \end{bmatrix} = \mathbf{C} \cdot \begin{bmatrix} p_{\Sigma 1} \\ p_{\Sigma 2} \\ p_{\Sigma 3} \end{bmatrix} \quad \begin{bmatrix} p_{\Delta\alpha} \\ p_{\Delta\beta} \\ p_{\Delta 0} \end{bmatrix} = \mathbf{C} \cdot \begin{bmatrix} p_{\Delta 1} \\ p_{\Delta 2} \\ p_{\Delta 3} \end{bmatrix}. \tag{20}$$

The following transformed power components result by replacing all voltages and currents by their $\alpha\beta 0$-components:

$$p_{\Sigma\alpha} = \frac{1}{2}u_e i_{e\alpha} - \frac{1}{2}u_0 i_{a\alpha} - \frac{1}{4}u_{a\alpha} i_{a\alpha} + \frac{1}{4}u_{a\beta} i_{a\beta} \quad (21)$$

$$p_{\Sigma\beta} = \frac{1}{2}u_e i_{e\beta} - \frac{1}{2}u_0 i_{a\beta} + \frac{1}{4}u_{a\alpha} i_{a\beta} + \frac{1}{4}u_{a\beta} i_{a\alpha} \quad (22)$$

$$p_{\Sigma 0} = \frac{1}{2}u_e i_{e0} - \frac{1}{4}(u_{a\alpha} i_{a\alpha} + u_{a\beta} i_{a\beta}) \quad (23)$$

$$p_{\Delta\alpha} = \frac{1}{2}u_e i_{a\alpha} - 2u_{a\alpha} i_{e0} - 2u_0 i_{e\alpha} - u_{a\alpha} i_{e\alpha} + u_{a\beta} i_{e\beta} \quad (24)$$

$$p_{\Delta\beta} = \frac{1}{2}u_e i_{a\beta} - 2u_{a\beta} i_{e0} - 2u_0 i_{e\beta} + u_{a\alpha} i_{e\beta} + u_{a\beta} i_{e\alpha} \quad (25)$$

$$p_{\Delta 0} = -2u_0 i_{e0} - u_{a\alpha} i_{e\alpha} - u_{a\beta} i_{e\beta}. \quad (26)$$

B. Energetic Analysis of the Arm Energies in Transformed Values for the Identification of the Balancing Currents

The mean value of each power component $\bar{p}_{\Sigma/\Delta\alpha/\beta/0}$ has to be zero for a symmetrical energy distribution in steady-state operation, according to the desired constant value of the arm energy $\bar{w}_C$, see (3). Therefore, the specific currents and voltages for a directed influence on the transformed arm energies have to be identified by these transformed power components of (21)–(26).

Here, two methods of energy balancing have to be distinguished depending on the frequency ω_a of the three-phase currents i_{ay}. If ω_a is high enough, which yields to the rotation of the phase angle by $\gamma_a = \omega_a \cdot t$ over the time t, only the mean values of the power components respectively the active power components have to be considered (high-frequency mode/hf mode). Consequently, the ac power components are buffered by the capacitors of the cells, which yields to the voltage pulsations $\tilde{u}_{Cxy}$ in the arms.

At lower output frequencies, the amount of the energy pulsation increases inversely proportional to ω_a [1]. Because of this, a compensation of the instantaneous power components in the arms, which are caused by the three-phase load, is needed (low-frequency mode/lf mode) [6], [7]. This allows the stable operation of the MMC even at standstill respectively at frequency $\omega_a = 0$.

1) Horizontal Balancing: The energy transfer between the three phases of the MMC for the balancing in horizontal direction, see Fig. 5, is achieved by the dc-components of the inner currents $i_{e\alpha\mathrm{DC}}$ and $i_{e\beta\mathrm{DC}}$. They generate together with the dc-voltage u_e active power components in $p_{\Sigma\alpha}$ and $p_{\Sigma\beta}$ according to (21) and (22), see Table I.

In each phase of the MMC occurs a dominant energy pulsation with the second harmonic of the output frequency ω_a. This power component could be compensated by additional inner ac currents $i_{e\alpha,hf2}$ and $i_{e\beta,hf2}$ for reducing the energy pulsation in the arms (hf2-mode), see [19]

$$i_{e\alpha\mathrm{AC2}} = \frac{1}{2u_e} \cdot \hat{u}_a \cdot \hat{i}_a \cdot \cos(2\gamma_a - \varphi_a) \quad (27)$$

$$i_{e\beta\mathrm{AC2}} = -\frac{1}{2u_e} \cdot \hat{u}_a \cdot \hat{i}_a \cdot \sin(2\gamma_a - \varphi_a). \quad (28)$$

TABLE I
OVERVIEW OF THE POWER COMPONENTS FOR BALANCING THE ARM ENERGIES IN TRANSFORMED VALUES

	power	voltage	current	frequency	comment
horizontal	$\bar{p}_{\Sigma\alpha}$	$u_e/2$	$i_{e\alpha DC}$	DC	
	$\bar{p}_{\Sigma\beta}$	$u_e/2$	$i_{e\beta DC}$	DC	
mean/total	$\bar{p}_{\Sigma 0}$	$u_e/2$	i_{e0DC}	DC	
vertical (hf)	$\bar{p}_{\Delta\alpha,hf}$	$\hat{u}_a$	$-\hat{i}_{ed-}$	ω_a	neg. seq.
	$\bar{p}_{\Delta\beta,hf}$	$\hat{u}_a$	$+\hat{i}_{eq-}$	ω_a	
	$\bar{p}_{\Delta 0,hf}$	$\hat{u}_a$	$-\hat{i}_{ed+}$	ω_a	pos. seq.
vertical	$\bar{p}_{\Delta\alpha/\beta/0,lf}$	$\hat{u}_0$	$\hat{i}_{e\alpha/\beta/0}$	ω_0	zero seq.

At low-output frequency or stationary space vectors ($\omega_a = 0$), the power components $-u_0 \cdot i_{a\alpha/\beta}$ and $\pm u_{a\alpha/\beta} \cdot i_{a\alpha/\beta}$ have to be compensated. This yields to the following internal dc-current components in the lf-mode:

$$i_{e\alpha\mathrm{DC}} = \frac{1}{2u_e}(u_{a\alpha} \cdot i_{a\alpha} - u_{a\beta} \cdot i_{a\beta} + 2u_{0a} \cdot i_{a\alpha}) \quad (29)$$

$$i_{e\beta\mathrm{DC}} = \frac{1}{2u_e}(-u_{a\alpha} \cdot i_{a\beta} - u_{a\beta} \cdot i_{a\alpha} + 2u_{0a} \cdot i_{a\beta}). \quad (30)$$

2) Mean Energy Control: The total energy stored in all cells of the MMC is influenced by the difference between the dc power and the 3ac active power P_a, see (23). The dc current for the power exchange with the dc-voltage source u_e will be without losses

$$i_{e0\mathrm{DC}} = \frac{1}{2u_e} \cdot \underbrace{(u_{a\alpha} \cdot i_{a\alpha} + u_{a\beta} \cdot i_{a\beta})}_{=\frac{2}{3}P_a} = \frac{1}{3} i_{e\mathrm{DC}}. \quad (31)$$

3) Vertical Balancing: The vertical balancing task ensures an energy equilibrium between the upper and lower arms of the MMC, see Fig. 5. The power components $\pm u_{a\alpha/\beta} \cdot i_{e\alpha/\beta}$ of (24)–(26) generate active power if the e-currents contain an ac current with the same frequency as $u_{a\alpha/\beta}$. These methods can be used in the hf-mode, if the output frequency is high enough.

The internal 3ac-current system is divided in its symmetrical components (positive and negative sequence components), [20], where $\mathbf{D}$ is the rotation matrix of (44) according to the phase angle γ_a

$$\begin{bmatrix} i_{e\alpha\mathrm{AC}} \\ i_{e\beta\mathrm{AC}} \end{bmatrix} = \underbrace{\mathbf{D}(\gamma_a) \cdot \begin{bmatrix} \hat{i}_{ed+} \\ \hat{i}_{\mathrm{eq}+} \end{bmatrix}}_{\mathrm{pos.seq.comp.}} + \underbrace{\mathbf{D}^{-1}(\gamma_a) \cdot \begin{bmatrix} \hat{i}_{ed-} \\ \hat{i}_{\mathrm{eq}-} \end{bmatrix}}_{\mathrm{neg.seq.comp}}. \quad (32)$$

The positive as well as the negative sequence components of the current system are expressed by their dq-components of the corresponding amplitudes. The mathematical analysis of the p_Δ-power components yields to the relations between the specific current components of (32) and the output voltage $\hat{u}_a$ for the corresponding power components $\bar{p}_{\Delta\alpha/\beta/0,hf}$, see Table I. The current component $i_{\mathrm{eq}+}$ causes only reactive power in the arms, so it is set to zero. At low-frequency operation (lf-mode), all power components p_Δ of (24)–(26) caused by the 3ac side have to be compensated. Corresponding active power components have to be independently generated by the common-mode voltage u_0 and the e-currents $i_{e\alpha/\beta/0}$. This is realized by the ac component u_{0e} according to (16) together with the three ac current

components $i_{e\alpha/\beta/0}$ at the same frequency and phase [6], [7], [21]

$$i_{e\alpha/\beta/0\mathrm{AC}} = \hat{i}_{e\alpha/\beta/0} \cdot \cos(\gamma_0). \tag{33}$$

The transformation of the $p_{\Delta\alpha/\beta}$ power of (21) and (25) delivers the values of the amplitudes for the internal currents at stationary space vectors for a balanced energy distribution in vertical direction

$$\hat{i}_{e\alpha} = \frac{1}{\hat{u}_{0e}} \cdot \Big(\frac{1}{2} u_e \cdot i_{a\alpha} - 2u_{a\alpha} \cdot i_{e0\mathrm{DC}} - 2u_{0a} \cdot i_{e\alpha\mathrm{DC}} - u_{a\alpha} \cdot i_{e\alpha\mathrm{DC}} + u_{a\beta} \cdot i_{e\beta\mathrm{DC}} \Big) \tag{34}$$

$$\hat{i}_{e\beta} = \frac{1}{\hat{u}_{0e}} \cdot \Big(\frac{1}{2} u_e \cdot i_{a\beta} - 2u_{a\beta} \cdot i_{e0\mathrm{DC}} - 2u_{0a} \cdot i_{e\beta\mathrm{DC}} + u_{a\alpha} \cdot i_{e\beta\mathrm{DC}} + u_{a\beta} \cdot i_{e\alpha\mathrm{DC}} \Big). \tag{35}$$

The $p_{\Delta 0}$ power of (26) causes a superposed ac component in the current of the dc side $i_{e\mathrm{DC}}$ respectively i_{e0}

$$\hat{i}_{e0} = \frac{1}{\hat{u}_{e0}} (-2u_{0\mathrm{DC}} \cdot i_{e0\mathrm{DC}} - u_{a\alpha} \cdot i_{e\alpha\mathrm{DC}} - u_{a\beta} \cdot i_{e\beta\mathrm{DC}}). \tag{36}$$

This ac current occurs only in the lf-mode and is comparatively small, but has to be tolerated by the dc-voltage source u_e.

IV. Control System of the MMC for Variable-Speed Drives

The complete control system for the MMC drive system is illustrated in Fig. 7. The six sums of the capacitor voltages u_{Cxy} of each arm as well as the six-arm currents i_{xy} are measured and transformed according to Section III-A to their related components, see Table I (here: $x \in \{u_C, i\}$)

$$\begin{bmatrix} x_{\Sigma\alpha} \\ x_{\Sigma\beta} \\ x_{\Sigma 0} \end{bmatrix} = \frac{1}{2}\mathbf{C} \cdot \begin{bmatrix} x_{p1}+x_{n1} \\ x_{p2}+x_{n2} \\ x_{p3}+x_{n3} \end{bmatrix} \quad \begin{bmatrix} x_{\Delta\alpha} \\ x_{\Delta\beta} \\ x_{\Delta 0} \end{bmatrix} = \mathbf{C} \cdot \begin{bmatrix} x_{p1}-x_{n1} \\ x_{p2}-x_{n2} \\ x_{p3}-x_{n3} \end{bmatrix}. \tag{37}$$

The five-current components are routed to their current controllers, which are described in Section II-D. The a-current controller of the three-phase machine receives its reference values in d- and q-components from its superposed speed controller. The machine model in the speed controller has to calculate the reference angle γ_a and the corresponding electrical frequency ω_a for the dq-current controller as well as for the phase angles of the internal ac balancing currents. The control voltages of the current controller are converted to the reference values of the arm voltages u^*_{xy} by the inverse transformation, see (14) and (15). The modulator (see block PWM in Fig. 7), which includes the cell balancing task, generates the pulse patterns for the transistors in the cells. The used modulation method is described in [7] and [10].

A. Switchover of the Current References

The current references have to be switched over between the lf- and hf-mode according to the generation of the active power components for the balancing tasks (see Table I). This is realized by a linear switchover between the effective current components

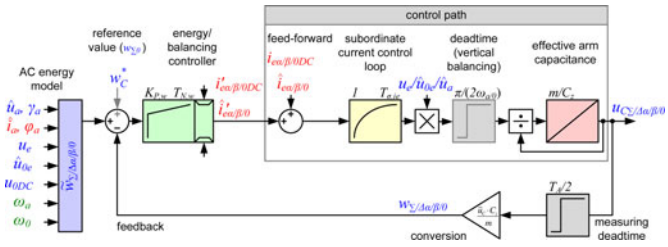

Fig. 8. Effective control loop for balancing the arm energies of the MMC.

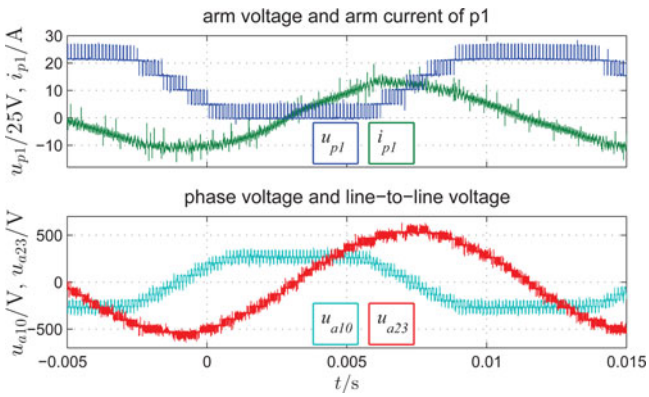

Fig. 9. Measured voltage and current waveforms of the MMC prototype.

depending on the weighting factors k_{lf} and k_{hf}. These factors are calculated by a linear relation to the electrical frequency ω_a

$$k_{hf}(\omega_a) = \begin{cases} 0 & \text{if } |\omega_a| \le \omega_{a1} \\ \dfrac{|\omega_a| - \omega_{a1}}{\omega_{a2} - \omega_{a1}} & \text{if } \omega_{a1} < |\omega_a| < \omega_{a2} \\ 1 & \text{if } \omega_{a2} \le |\omega_a| \end{cases} \tag{38}$$

$$k_{lf}(\omega_a) = 1 - k_{hf}(\omega_a). \tag{39}$$

The frequencies ω_{a1} and ω_{a2} define the range of the linear switchover. The three reference values of the dc and internal currents $i^*_{e\alpha/\beta/0}$ are calculated as illustrated in Fig. 6. Here, the feed-forward values of (29)–(31) and (34)–(36), the parts from the subordinated energy, and balancing controllers (ac: $\hat{i}'_{e\alpha/\beta/0}$, dc: $i'_{e\alpha/\beta/0\mathrm{DC}}$), as well as the components for the reduction of the pulsating energy in the hf2-mode [$i_{e\alpha/\beta\mathrm{AC}2}$, see (27) and (28)] are joined and switched over [8].

B. Control of Arm Energies

The resulting control loops for balancing the arm energy components $w_{\Sigma/\Delta\alpha/\beta/0}$ according to their six transformed power values of (20) are shown in Fig. 8. The several controllers are designed based on these control loops, which include the transfer functions of the relevant components. The measured and transformed voltages $u_{C\Sigma/\Delta\alpha/\beta/0}$ are converted in their arm energies, comparable to (3). The reference value of the total energy controller ($w_{\Sigma 0}$) is calculated by the desired mean voltage of the

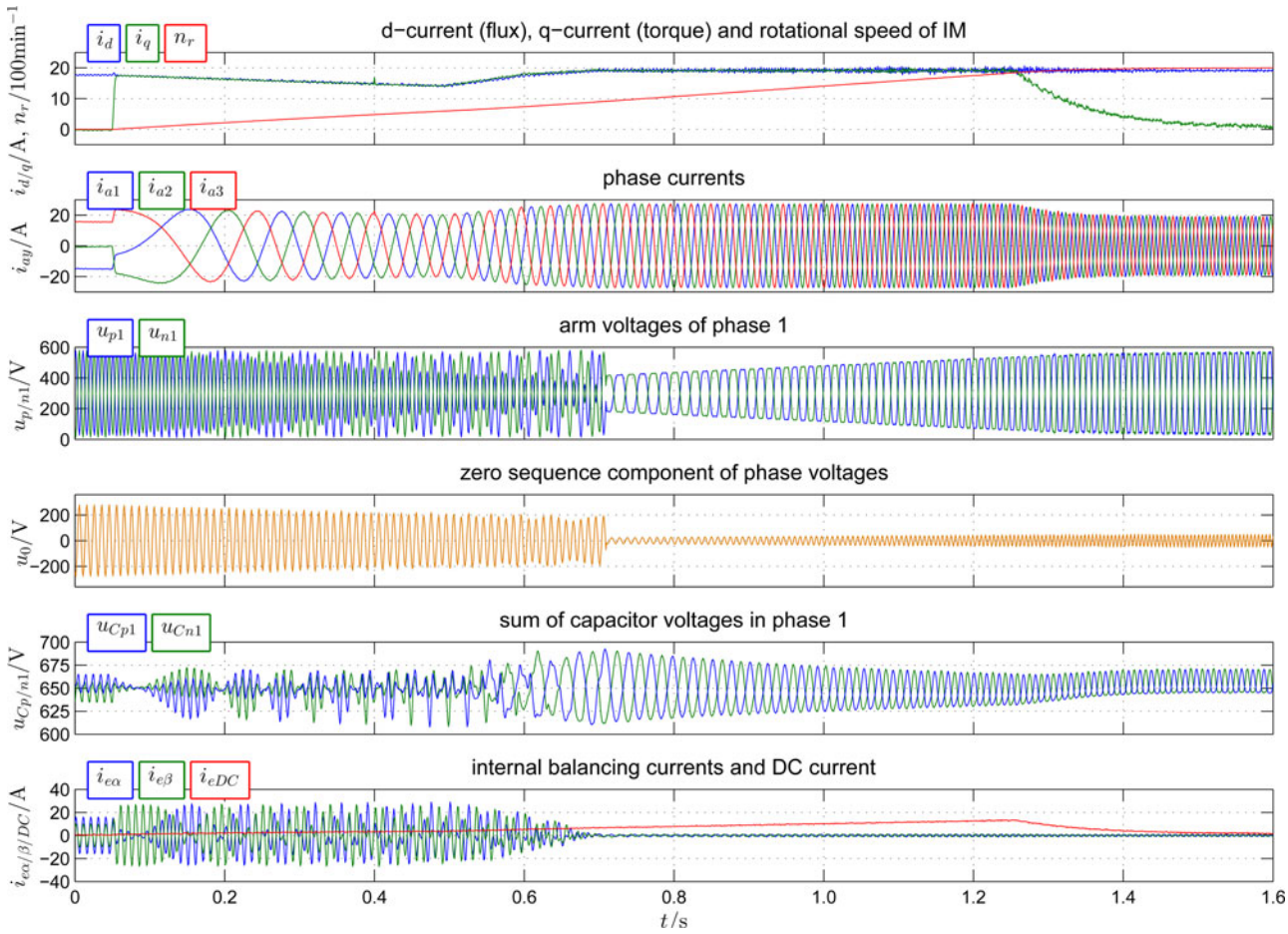

Fig. 10. Run-up of a field-oriented controlled induction machine fed by the MMC prototype, short time averaged values at $T_A = 1/f_{\mathrm{PWM}} = 1/(8\,\mathrm{kHz})$.

arms $\bar{u}_C$

$$w_C^* = \frac{\bar{u}_C^2 \cdot C_z}{m} = 2\bar{w}_C. \tag{40}$$

This reference value is twice the desired mean values $\bar{w}_C$ of the arm energies, due to the calculation in transformed values. The mean value of the references of the other five balancing controllers have to be zero to achieve a symmetrical energy distribution in the arms. The ac content of the arm energies $\tilde{w}_{xy}$ respectively their transformed components would cause several ac currents in the corresponding currents (compare to [8], where filters in the feedback are used). To avoid this issue, the pulsating parts of the energies are calculated by an ac energy model on the basis of the measured currents, reference voltages, frequencies, and phase angles, see Fig. 8. In contrast to the analysis of the active power components in Section III-A, these reactive power components are calculated by the integration of the ac power components of (21)–(26) to their respective instantaneous values of the time-variant energies $\tilde{w}_{\Sigma/\Delta\alpha/\beta/0}$.

The maximum gain $K_{P,w\Sigma}$ of the energy controller ($w_{\Sigma 0}$) and the horizontal balancing controllers ($w_{\Sigma\alpha/\beta}$) is estimated compared to the design of the current controllers

$$K_{P,w\Sigma} = \frac{1}{u_e \cdot (\frac{T_A}{2} + T_{\sigma,ie})}. \tag{41}$$

In the vertical balancing control loops, the different voltages of $\hat{u}_a$ and $\hat{u}_0$, as well as the dominant mean dead time due to the generation of the active power by the ac voltages and currents have to be included in the gain of the controllers

$$K_{P,w\Delta} = \frac{1}{\pi} \cdot \left(k_{hf} \cdot \frac{|\omega_a|}{\hat{u}_a} + k_{lf} \cdot \frac{|\omega_0|}{\hat{u}_0} \right). \tag{42}$$

An additional integral part of the controller could be used to improve the tracking performance at steady-state operation.

The amplitude $\hat{u}_0$ of the common-mode voltage for the vertical balancing in the lf-mode is calculated on the basis of the residual part of the arm voltages u_{xy}. Here, the voltages $u_{L\alpha/\beta/0}$ for the e-current control are subtracted in consideration of the necessary voltage amplitude $\hat{u}_a$ for the machine and the overmodulation by u_{0a} according to (16), which yields to the limits $u_{ay0,\max}$ and $\hat{u}_{a,\max}$ in Fig. 7.

V. Prototype and Measurements

The process of the dimensioning of the MMC regarding the necessary cell capacitance C_z for buffering the pulsating energies in the arms as well as the resulting current stress are extensively described in [10], [22], and [23]. A low-voltage MMC

prototype, see [9] and [11], is designed based on these fundamentals to demonstrate the effectiveness of the control system for feeding three-phase machines. It consists of $m=5$ cells per arm with the maximum cell voltage of $u_{Cxyz,\max}=150$ V and the cell capacitance of $C_z=4400\,\mu$F. The MMC is supplied by a voltage source with $u_e=600$ V and feeds a 15-kW three-phase induction machine. The reference voltage of the energy controller is set to $\bar{u}_C=650$ V.

The measurements in Fig. 9 of the arm voltage u_{p1}, of the corresponding arm current i_{p1}, as well as the voltage waveforms on the 3ac-side at the hf-mode demonstrate the high-quality waveforms with very low-harmonic content.

The run-up of the field-orientated controlled induction machine is illustrated in the measurements of Fig. 10. The machine is magnetized by i_d and a step in the torque is initiated by i_q at $t=0.05$ s. The fast dynamic response of the controlled MMC after this step causes no overshoot, neither in the currents nor in the capacitor voltages u_{Cxy}. During the low-speed operation of the machine, the MMC is balanced by the lf-mode until the mode is switched to the hf-mode in the range of $t\approx[0.5..0.7]$s. This is visible on the significant ac component of the common-mode voltage u_0 and the corresponding inner balancing currents $i_{e\alpha/\beta}$. The magnitude of the energy pulsation in the lf-mode can be freely adjusted by ω_0. The choice of $\omega_0=2\pi\times 100$ Hz causes the desired effect in the capacitor voltages u_{Cxy} to keep them in the allowable range around the desired mean value of $\bar{u}_C=650$ V. The phase currents i_{ay} respectively i_q and i_d are reduced during the lf-mode to keep the inner balancing currents $i_{e\alpha/\beta}$ and, therefore, the arm currents i_{xy} in acceptable limits. This is necessary, because the MMC is dimensioned on the basis of the current stress at the nominal operating point. During the switchover between the lf- and hf-mode, the motor currents are increased to their nominal values, because the additional current stress of the inner currents is decreased to nearly zero. The switchover between the lf- and hf-mode is set in the range of $\omega_{a1}=2\pi\times 20$ Hz and $\omega_{a2}=2\pi\times 30$ Hz. In the hf-mode, only a very small current ripple remains in the internal balancing currents due to the simplification of the calculated arm energies, where the control voltages are neglected. The dc-current $i_{e\mathrm{DC}}$ obviously contains no ac component not even in the lf-mode.

VI. Conclusion

A cascaded control system for the MMC to feed variable-speed drives is derived on the base of the analysis of the equivalent circuit as well as of the active power components in the arms. The realization by the transformation of all relevant values allows a dynamic control of the arm energies over the complete operation range of the drive at minimum internal currents. The systematical design process of the several controllers and feed-forward components for the balancing tasks are presented. Finally, the measurement at a MMC prototype combined with a field-oriented control of an induction machine validates the approach and illustrates the performance of the control system. The proposed control and balancing system of the MMC allows the supply of three-phase machines independent of their type and motor control system.

Appendix

Clarke-transformation with matrix $\mathbf{C}$

$$\begin{bmatrix} y_\alpha \\ y_\beta \\ y_0 \end{bmatrix} = \mathbf{C}\cdot\begin{bmatrix} x_1 \\ x_2 \\ x_3 \end{bmatrix} = \begin{bmatrix} \frac{2}{3} & -\frac{1}{3} & -\frac{1}{3} \\ 0 & \frac{1}{\sqrt{3}} & -\frac{1}{\sqrt{3}} \\ \frac{1}{3} & \frac{1}{3} & \frac{1}{3} \end{bmatrix}\cdot\begin{bmatrix} x_1 \\ x_2 \\ x_3 \end{bmatrix} \tag{43}$$

rotation matrix $\mathbf{D}(\gamma)$

$$\mathbf{D}(\gamma) = \begin{bmatrix} \cos(\gamma) & -\sin(\gamma) \\ \sin(\gamma) & \cos(\gamma) \end{bmatrix}. \tag{44}$$

References

[1] R. Marquardt, A. Lesnicar, and J. Hildinger, "Modulares Stromrichterkonzept für Netzkupplungsanwendungen bei hohen Spannungen," presented at the ETG-Fachtagungen, Bad Nauheim, Germany, 2002.

[2] M. Hiller, D. Krug, R. Sommer, and S. Rohner, "A new highly modular medium voltage converter topology for industrial drive applications," in *Proc. 13th Eur. Conf. Power Electron. Appl.*, 2009, pp. 1–10.

[3] M. Hagiwara, K. Nishimura, and H. Akagi, "A modular multilevel PWM inverter for medium-voltage motor drives," in *Proc. IEEE Energy Convers. Congr. Expo.*, 2009, pp. 2557–2564.

[4] M. Hagiwara, K. Nishimura, and H. Akagi, "A Medium-Voltage Motor Drive With a Modular Multilevel PWM Inverter," *IEEE Trans. Power Electron.*, vol. 25, no. 7, pp. 1786–1799, Jul. 2010.

[5] A. Antonopoulos, K. Ilves, L. Angquist, and H.-P Nee, "On interaction between internal converter dynamics and current control of high-performance high-power AC motor drives with modular multilevel converters," in *Proc. IEEE Energy Convers. Congr. Expo.*, 2010, pp. 4293–4298.

[6] A. Korn, M. Winkelnkemper, and P. Steimer, "Low output frequency operation of the Modular Multilevel Converter," in *Proc. IEEE Energy Convers. Congr. Expo.*, 2010, pp. 3993–3997.

[7] J. Kolb, F. Kammerer, and M. Braun, "A novel control scheme for low frequency operation of the Modular Multilevel Converter," in *Proc. Power Electron., Intell. Motion Energy Manag. Eur.*, 2011, pp. 977–982.

[8] J. Kolb, F. Kammerer, and M. Braun, "Straight forward vector control of the Modular Multilevel Converter for feeding three-phase machines over their complete frequency range," in *Proc. 37th Annu. Conf. IEEE Ind. Electron. Soc.*, 2011, pp. 1596–1601.

[9] J. Kolb, F. Kammerer, P. Grabherr, M. Gommeringer, and M. Braun, "Boosting the efficiency of low voltage modular multilevel converters beyond 99%," in *Proc. Power Electron., Intell. Motion Energy Manag. Eur.*, 2013, pp. 1157–1164.

[10] J. Kolb, F. Kammerer, and M. Braun, "Dimensioning and design of a Modular Multilevel Converter for drive applications," in *Proc. 15th Int. Power Electron. Motion Contr. Conf.*, 2012, pp. LS1a-1.1-1–LS1a-1.1-8.

[11] J. Kolb, F. Kammerer, and M. Braun, "Operating performance of modular multilevel converters in drive applications," in *Proc. Power Electron., Intell. Motion Energy Manag. Eur.*, Nuremberg, Germany, 2012, pp. 583–590.

[12] A. Antonopoulos, L. Angquist, S. Norrga, K. Ilves, and H.-P. Nee, "Modular multilevel converter ac motor drives with constant torque form zero to nominal speed," in *Proc. IEEE Energy Convers. Congr. Expo.*, 2012, pp. 739–746.

[13] M. Hagiwara, I. Hasegawa, and H. Akagi, "Start-up and low-speed operation of an electric motor driven by a modular multilevel cascade inverter," *IEEE Trans. Ind. Appl.*, vol. 49, no. 4, pp. 1556–1565, Jul./Aug. 2013.

[14] J.-J. Jung, H.-J. Lee, and S.-K. Sul, "Control strategy for improved dynamic performance of variable-speed drives with the modular multilevel converter," in *Proc. IEEE Energy Convers. Congr. Expo.*, 2013, pp. 1481–1488.

[15] S. Rohner, S. Bernet, M. Hiller, and R. Sommer, "Analysis and simulation of a 6 kV, 6 MVA modular multilevel converter," in *Proc. IEEE 35th Annu. Ind. Electron. Conf.*, 2009, pp. 225–230.

[16] S. Rohner, S. Bernet, M. Hiller, and R. Sommer, "Modulation, losses, and semiconductor requirements of modular multilevel converters," *IEEE Trans. Ind. Electron.*, vol. 57, no. 8, pp. 2633–2642, Aug. 2010.

[17] Q. Tu, Z. Xu, H. Huang, and J. Zhang, "Parameter design principle of the arm inductor in modular multilevel converter based HVDC," in *Proc. Int. Conf. Power Syst. Technol.*, 2010, pp. 1–6.

[18] D. Schröder, *Elektrische Antriebe—Regelung von Antriebssystemen*. New York, NY, USA: Springer-Verlag, 2009.
[19] S. Engel and R. De Doncker, "Control of the modular multi-level converter for minimized cell capacitance," in *Proc. 14th Eur. Conf. Power Electron. Appl.*, 2011, pp. 1–10.
[20] P. Munch, D. Gorges, M. Izak, and S. Liu, "Integrated current control, energy control and energy balancing of Modular Multilevel Converters," in *Proc. 36th Annu. Conf. IEEE Ind. Electron. Soc.*, 2010, pp. 150–155.
[21] K. Wang, Y. Li, Z. Zheng, and L. Xu, "Voltage fluctuation suppression method of floating capacitors in a new modular multilevel converter," in *Proc. IEEE Energy Convers. Congr. Expo.*, 2011, pp. 2072–2078.
[22] M. Spichartz, V. Staudt, and A. Steimel, "Analysis of the module-voltage fluctuations of the modular multilevel converter at variable-speed drive applications," in *Proc. 13th Int. Conf. Optim. Electr. Electron. Equipment*, 2012, pp. 751–758.
[23] L. Harnefors, S. Norrga, A. Antonopoulos, and H.-P. Nee, "Dynamic modeling of modular multilevel converters," in *Proc. 14th Eur. Conf. Power Electron. Appl.*, 2011, pp. 1–10.

Johannes Kolb was born in Pforzheim, Germany, in 1982. He received the Dipl.-Ing. degree from the University of Karlsruhe, Karlsruhe, Germany, in 2007.

From 2007 to 2013, he was with the Elektrotechnisches Institut, Karlsruhe Institute of Technology (KIT), Karlsruhe, Germany, where he was engaged in the research of power electronics especially multilevel converters. Since 2013, he has been the Team Leader of the Working Group Electric Drives at the Schaeffler Hub for Automotive Research in E-Mobility at the KIT.

Felix Kammerer was born in Schramberg, Germany in 1982. He received the Dipl.-Ing. degree from the Karlsruhe Institute of Technology (KIT), Karlsruhe, Germany, in 2010. He is currently working toward the Ph.D. degree with the Elektrotechnisches Institut, Karlsruhe Institute of Technology, Germany.

Since 2010, he has been working as a Research Engineer with the Elektrotechnisches Institut, KIT. His research interests include power electronics and electrical drives, especially modular multilevel converters and their corresponding control systems.

Mario Gommeringer was born in Radolfzell am Bodensee, Germany, in 1983. He received the Dipl.-Ing. degree from the University of Karlsruhe, Karlsruhe, Germany, in 2009.

From 2009 to 2011, he was an Engineer in an industrial company. Since 2011, he has been with the Elektrotechnisches Institut, Karlsruhe Institute of Technology, Karlsruhe, Germany. His research interests include multilevel converters and novel converter topologies.

Michael Braun received the Dipl.-Ing. and Dr.-Ing. degrees from the Technische Hochschule Darmstadt, Germany, in 1978 and 1983, respectively.

From 1983 to 1994, he was with Siemens AG, Erlangen, Germany, where he was engaged in the development of power electronics and electrical drives. Since 1994, he has been a Professor and the Head of the Elektrotechnisches Institut, Karlsruhe Institute of Technology, Karlsruhe, Germany. His research interests include power electronics, control of electrical drives, and mechatronics.